JOURNAL OF OPTOELECTRONICS AND ADVANCED MATERIALS, Vol. 11, No. 11, November 2009, p. 1848 - 1854

Electrodeposited hydroxyapatite thin films modified by ion beam irradiation

M. S. DJOŠIĆ[a], N. BIBIĆ[b], M. N. MITRIĆ[b], M. ŠILJEGOVIĆ[b], J. N. STOJANOVIĆ[a], B. JOKIĆ[c], Dj. T. JANAĆKOVIĆ[c], V. B. MIŠKOVIĆ-STANKOVIĆ[c,*]
[a]*Institute for Technology of Nuclear and Other Mineral Raw Materials, Franse d'Epere 86, 11000 Belgrade, Serbia*
[b]*Institute of Nuclear Sciences "Vinča", P.O.Box 522, 11001 Belgrade, Serbia*
[c]*Faculty of Technology and Metallurgy, University of Belgrade, Karnegijeva 4, P.O.Box 3503, 11120 Belgrade, Serbia*

Surface modification of hydroxyapatite (HA) thin films electrodeposited on titanium was conducted by ion implantation, using nitrogen and argon ions at different constant fluences of $1x10^{15}$, $1x10^{16}$ and $1x10^{17}$ ions/cm^2. SEM and XRD analysis, as well as SRIM calculation, were used to monitor the changes induced by ion bombardment. In the case of HA film implanted with N^{4+} ions, the unit cell parameters and unit cell volume increase with increasing nitrogen ion fluences. Similarly, the unit cell parameters and unit cell volume increase after Ar^{6+} ions irradiation to a $1x10^{15}$ ions/cm^2. At higher fluences, the unit cell parameters and unit cell volume decrease when argon ion fluences increase to $1x10^{16}$ and $1x10^{17}$ ions/cm^2. These structural changes are consequence of different mechanism of energy transfer of nitrogen and argon ions to HA film. For nitrogen ion irradiation electron energy loss is predominant, while for argon ion irradiation nuclear energy transfer to HA film prevails.

(Received October 31, 2009; accepted November 23, 2009)

Keywords: Films; Surfaces; Hydroxyapatite; Ion implantation

1. Introduction

Titanium and some of its alloys are the most often the material of choice for implants due to their mechanical strength [1]. Implants are retired in the corrosive environment of the human body for long periods of time. The biocompatibility and corrosion resistance of these implants are primary determined by their constituent material and surface microstructural properties such as roughness, grain size, etc. Surface stabilization of biomedical implants by different methods (e.g. coating with materials with good biocompatibility) can be used for controlling the corrosion resistance of the implant materials. Thin films of bioactive materials such as hydroxyapatite (HA), are attractive as bioceramic films [2]. In the past decade, several methods have been reported to deposit HA onto implant surfaces [3-10]. The advantages of electrophoretic deposition method [11-17] are the low operating temperature as well as the possibility of the coating thickness and morphology controlling through adequate conditions of the process.

Surface modification by ion beam irradiation method has been identified as a good technique to improve bioactivity of HA [18-20] and its mechanical properties [21,22], and to reduce particle size [19], without detrimentally affecting bulk properties. Namely, the surface modification induced by irradiation can give the bioactive materials of improved ion-exchange properties depending upon the particular material and the type of ions used. This can be controlled by: (a) varying the depth to which the ions penetrate by varying the energy of ion bombardment or the angle of the material surface related to the ion beam; (b) varying the dose (or ions per unit area) of the ion beam; and (c) varying the type and combination of ions used.

Led by these considerations, we have carried out a series of experiments, in which hydroxyapatite thin films electrodeposited on titanium were implanted with N^{4+} and Ar^{6+} ions. The aim of this work was to qualitatively explain the mechanism of HA surface modification after irradiation with N^{4+} and Ar^{6+} ions.

2. Experimental

2.1. Synthesis of hydroxyapatite powder

Synthesis of HA powder were performed by dissolving of 0.55 g $CaCl_2$, 0.74 g $Na_2H_2EDTA{\cdot}2H_2O$, 0.6 g NaH_2PO_4 and 0.6 g urea (all reagents p.a. grade, Merck) in 100 ml of distilled water. The solution was annealed at 160 °C during 3 h in sealed tube. The particles were further washed with distilled water and dried at 105 °C during 2 h.

For the preparation of HA suspension, 1.0 g of HA powder was added into 100 ml of ethanol. With the aim to increase the stability of suspension, the 55 µl of 10 wt.% HCl was added. Then, the suspension was treated by an ultrasonically treatment for 30 min.

2.2. Electrophoretic deposition of hydroxyapatite films on titanium from ethanol suspension

A two-electrode cell arrangement was used for cathodic electrodeposition. The working electrode was a

titanium plate (8 mm x 12 mm x 0.127 mm, Ti 99.7 %, ALDRICH). The counter electrode was platinum panel, placed parallel to the working electrode at a distance of 1.5 cm. The titanium plates were degreased in acetone and then in ethanol for 15 min in ultrasonic bath.

Hydroxyapatite films were deposited on titanium from ethanol HA suspension using the constant voltage method. The experiments were performed at constant voltage of 30 V at room temperature, while deposition time was 30 s. The hydroxyapatite deposit mass, determined by weighing the cathode before and after deposition, was calculated to be 1.30 mg.

2.3. Ion-implantation of hydoxyapatite films electrodeposited on titanium

The ion implantation experiments were conducted at the L3A Channel for materials modification (Institute of Nuclear Sciences "Vinča", Belgrade), which is directly connected to the Ion Source (mVINIS). The target chamber is $1\times1\times1$ m^3 vacuum vessel, with a target holder located in the central position. The target holder is a water-cooled disk, 300 mm in diameter, that enables positioning and rotation of the samples in order to expose their surface towards the ion beam from the mVINIS, the low energy ion beam from the argon gun, or the electron-beam evaporator (e-gun).

Two sets of experiments were performed: by implantation of N^{4+} ions into HA films electrodeposited on titanium (set A), and by implantation of Ar^{6+} ions into HA films (set B). The implantation was carried out at a three different constant fluences of $1x10^{15}$, $1x10^{16}$ and $1x10^{17}$ ions/cm^2 with energies of 60 keV and 90 keV, for nitrogen and argon ions, respectively. All irradiations were performed at room temperature and the implanted area was homogeneously covered by means of an x-y sweeping system. The beam current was maintained at around 0.05 μA cm^{-2} for the Ar^{6+} and N^{4+} ions. During the each set of implantation experiments, the one sample was exposed to vacuum, but not implanted, with the aim to be used for comparing the results. The color of hydroxyapatite films was not change during the implantation.

2.4. Characterization of hydroxyapatite powder, non-implanted and implanted hydoxyapatite films electrodeposited on titanium

HA powder and HA films non-implanted and implanted with N^{4+} and Ar^{6+} ions, were structurally characterized by X-ray powder diffraction (XRPD) theta-theta diffractometer (BRUKER D8, Karlsruhe, Germany). The XRPD experiments were performed in asymmetrical reflection parallel beam mode (with incident beam angle of 3°) with CuKα radiation (1.5418 Å) using Gobel Mirror bent gradient multilayer optics. The scattered intensities were measured with a scintillation counter. The angular range was from 8° to 80° with the steps of 0.05° and the measuring time was 5 s per step at room temperature.

The microstructure of HA powder was characterized by scanning electron microscopy (SEM) using a JEOL T-20 instrument, operated at 19 kV. The microstructure of the HA films was studied by scanning electron microscopy SEM using a JSM-35 (JEOL) operated at 25 kV. The micrographs were taken at 0^o, and the contrast in micrographs is due to the difference in secondary electron yields (SE mode).

In order to study the influence of the implantation and ions penetration into HA films, the ion ranges and distributions were calculated by the SRIM (Stopping and Range of Ions in Matter) code [23]. For nitrogen (energy 60 keV) and argon (energy 90 keV) ions, the ion ranges, R_p, and associated statistical spread - standard deviation, ΔR_p, as well as the electron energy loss $(dE/dx)_e$ and nuclear energy loss $(dE/dx)_n$ were obtained. Then, the irradiation energies were chosen in such a way that the average projected ranges of the ions were inside HA films and close to the surface of the film, according to simulations done with the SRIM code.

3. Results and discussion

3.1. Hydroxyapatite powder and non-implanted hydroxyapatite films

Fig. 1 represents the XRD pattern of the HA powder (Card JCPDS No. 09-0432). The crystallite domain size from the (002) reflection was calculated to be 43.4 nm, using software WinFit [24].

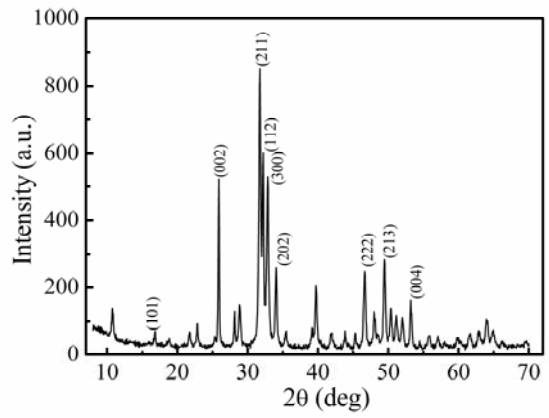

Fig. 1. XRD pattern of HA powder.

Fig. 2 shows the SEM micrograph of HA powder. It can be observed that HA particles are spherical and each particle consists of great number of agglomerated nanosized subparticles. Namely, the crystallite domain size for HA powder from the (002) reflection was calculated to be 43.4 nm. SEM micrograph (Fig. 2.) represents the spherical HA particles, having the size in the range of 1-3 μm. This indicates that agglomerates were formed through the drying process. This proposition is in good agreement with the literature where the nucleation-aggregation-agglomeration-growth mechanism is proposed [25].

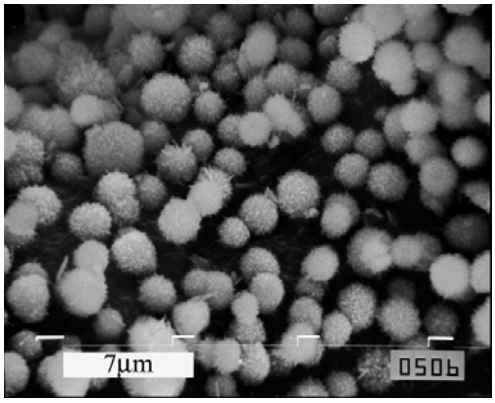

Fig. 2. SEM micrograph of HA powder.

Fig. 3 represents the XRD pattern of non-implanted HA film electrodeposited on titanium. Peaks for HA and titanium (originated from the substrate) are identified. Comparison of Fig. 3 and Fig. 1 suggests that during electrophoretic deposition process crystal structure of HA powder was not changed.

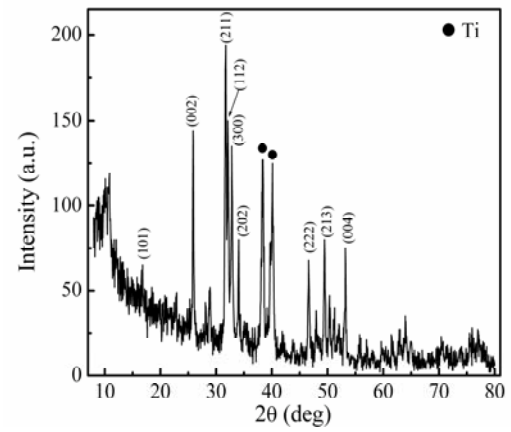

Fig. 3. XRD pattern of non-implanted HA film electrodeposited on titanium.

The SEM micrograph of non-implanted HA film (Fig. 4) represents the homogenous, crack-free structure of HA film obtained by electrodeposition process.

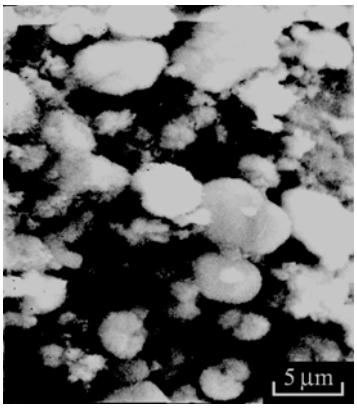

Fig. 4. SEM micrograph of non-implanted HA film.

3.2 Hydroxyapatite films implanted with N^{4+} and Ar^{6+} ions

The HA films implanted with N^{4+} and Ar^{6+} at different fluences of $1x10^{15}$, $1x10^{16}$ and $1x10^{17}$ ions/cm^2 were characterized by XRD and SEM analysis, while SRIM calculation was used for determination of ion penetration into HA films.

SRIM calculation was performed for nitrogen and argon ions with energies of 60 keV and 90 keV, respectively, implanted into HA films. Besides, the density of HA film was used (3.06 g cm^{-3}). Consequently, the values of estimated ion ranges, R_p, statistical spread-standard deviation, ΔR_p and electron energy loss $(dE/dx)_e$ and nuclear energy loss $(dE/dx)_n$, for nitrogen and argon ions are given in Table 1.

Table 1. Summary of the calculated values of ion ranges, R_p, statistical spread-standard deviation, ΔR_p, electron energy loss $(dE/dx)_e$ and nuclear energy loss $(dE/dx)_n$, for nitrogen and argon ions

Ion	N^{4+}	Ar^{6+}
Energy (keV)	60	90
R_p (nm)	134	78
ΔR_p (nm)	47	20
$(dE/dx)_e$ (eV/nm)	$2.6x10^2$	$3.2x10^2$
$(dE/dx)_n$ (eV/nm)	$1.1 x10^2$	$6.7x10^2$

The results clearly show that argon ions will penetrate into HA film less than nitrogen ions. Whereas the nitrogen range distribution is determined by electronic stopping, that of argon ions is determined by nuclear loss. It can be said that argon slows down and undergoes more frequent nuclear collisions, indicating that the heavier ions (Ar) induces much larger energy deposition density than lighter (N) ions [26]. The distribution of the displaced target atoms for argon ion implantation is considerably larger than that for nitrogen implantation into HA films. Consequently, the surface erosion of HA films by electronic energy loss (N ions irradiation) seems to be absent and only erosion by elastic collision between the projectiles and near surface atoms contribute (collisional sputtering). Explicitly, the sputtering coefficient is more pronounced for argon ion irradiation (2.3 at/ion comparing to 0.43 at/ion for nitrogen ion), as calculated by the SRIM code.

In addition, ion beams can alter the topography of surfaces on which they impinge [27,28]. SEM was used for the analysis of surface topography of HA films before and after implantation with nitrogen and argon ions. Figs. 5a-c show the SEM micrographs of HA surface after irradiation with 60 keV N^{4+} ions at fluences of $1x10^{15}$ ions/cm^2, $1x10^{16}$ ions/cm^2 and $1x10^{17}$ ions/cm^2, respectively. No changes of the surface topography after nitrogen implantation as compared to non-implanted sample (Fig. 4) were observed. It is evident that the development of the surface topography during nitrogen implantation is negligible. On the other hand, the results show that implantation with argon ions alters the topography of the HA surface. The SEM micrographs shown in Figs. 6a-c were taken from the samples

implanted with 90 keV Ar^{6+} ions at fluences of $1x10^{15}$ ions/cm^2, $1x10^{16}$ ions/cm^2 and $1x10^{17}$ ions/cm^2, respectively. The surface topography was not changed significantly by argon ions implantation at lower fluences (Fig. 6a and b). A slightly higher surface roughness can be noticed compared with the non-implanted sample. On the other hand, the surface topography was changed significantly by argon ions implantation at higher argon ion fluence ($1x10^{17}$ ions/cm^2), as shown in Fig. 6c. A more pronounced surface topography was developed and formation of cone-like structure occurred. The observed cone-like shapes are denoted by arrows in Fig. 6c. This is due to the sputtering effects of argon ions during interaction with HA films. Thus, the main route of surface modification of HA films is a consequence of Ar ions induced damage and surface erosion.

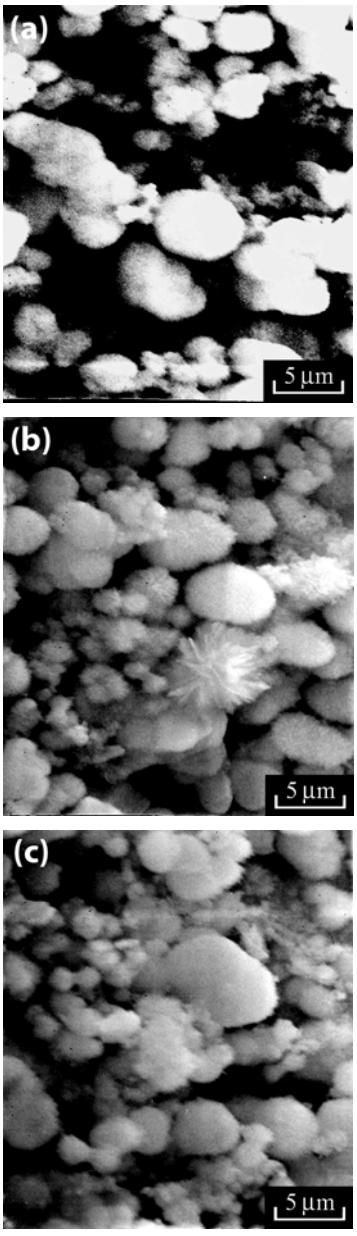

Fig. 5. SEM micrographs of HA films implanted with nitrogen ions at fluences of (a) $1x10^{15}$ ions/cm^2, (b) $1x10^{16}$ ions/cm^2, and (c) $1x10^{17}$ ions/cm^2.

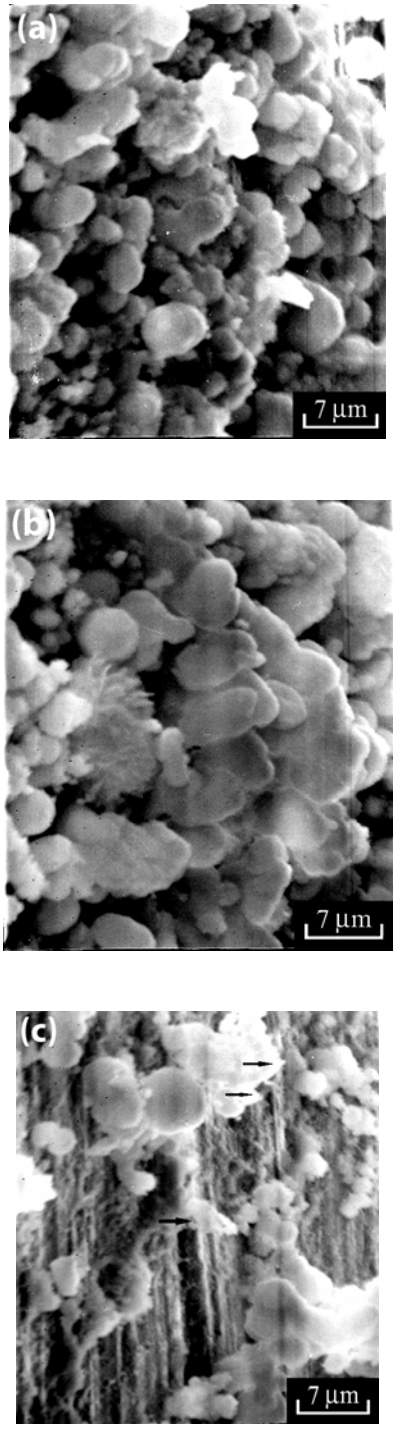

Fig. 6. SEM micrographs of HA films implanted with argon ions at fluences of (a) $1x10^{15}$ ions/cm^2, (b) $1x10^{16}$ ions/cm^2, and (c) $1x10^{17}$ ions/cm^2.

Figs. 7 and 8 represent the XRD patterns of HA films electrodeposited on titanium after implantation by different fluences of N^{4+} and Ar^{6+} ions, respectively. The X-ray diffraction pattern corresponding to HA phase was recorded for both non-implanted (Fig. 3) and implanted films (Figs. 7 and 8). The initial crystalline structure of HA films was preserved after ion implantation.

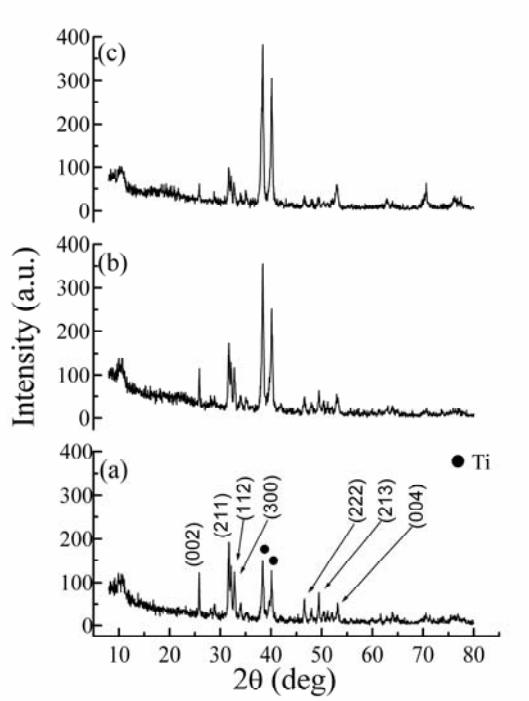

Fig. 7. XRD patterns of HA films implanted with nitrogen ions at fluences of (a) 1x10^{15} ions/cm^2, (b) 1x10^{16} ions/cm^2, and (c) 1x10^{17} ions/cm^2.

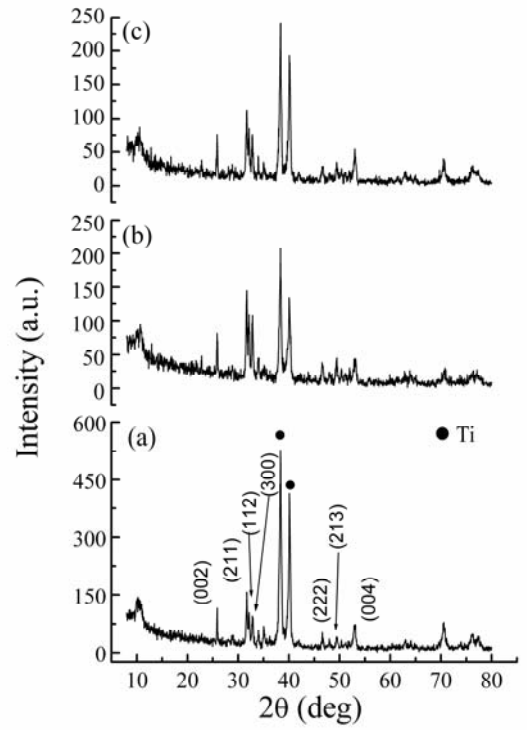

Fig. 8. XRD patterns of HA films implanted with argon ions at fluences of (a) 1x10^{15} ions/cm^2, (b) 1x10^{16} ions/cm^2, and (c) 1x10^{17} ions/cm^2.

The effect of ion fluences on the relative intensities of XRD reflection at $2\theta = 26°$ of implanted HA films can be noticed in Fig. 9a, for implantation with nitrogen ions and in Fig. 9b, for implantation with argon ions.

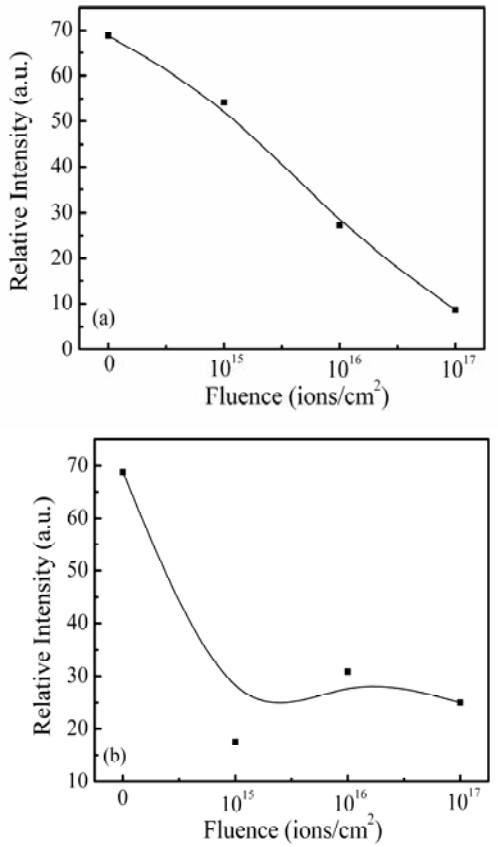

Fig. 9.The effect of ion fluences on relative intensities of XRD reflection at $2\theta = 26°$ of (a) HA films implanted with nitrogen ions, and (b) HA films implanted with argon ions.

Fig. 10 shows the dependence of crystallite domain size for (002) plane on fluences of implanted N^{4+} and Ar^{6+} ions. The crystallite domain size from the (002) reflection was calculated using software WinFit [24]. The increase in applied fluences decreases the HA crystallite domain size for both implanted ions.

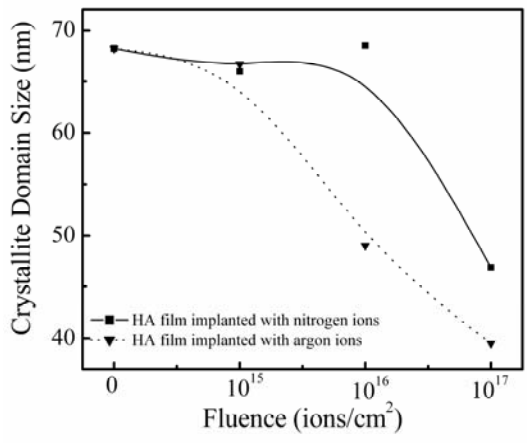

Fig. 10. Dependence of crystallite domain size for (002) plane on fluences of implanted nitrogen and argon ions.

It can be observed from Fig. 9a that relative intensities of the reflection at $2\theta = 26°$ decrease with increasing nitrogen ion fluence. This behavior indicates that the decrease in crystallinity of HA film, as well as the decrease in crystallite domain size (Fig. 10), are the consequence of electron energy loss mechanism. This is in accordance with the results from literature [19,29] which confirmed that energy transfer promoted the decrease in crystallinity.

Fig. 9b shows that relative intensities of the reflection at $2\theta = 26°$ decrease after Ar^{6+} ions irradiation to a $1x10^{15}$ ions/cm^2. At higher fluences, the relative intensities slightly increase when argon ion fluences increase to $1x10^{16}$ and $1x10^{17}$ ions/cm^2. These structural changes, i.e. decrease in crystallinity of HA film followed by further increase, as well as the decrease in crystallite domain size (Fig. 10), can be due to the fact that nuclear energy loss dominates for argon ions irradiation. At lower fluences the decrease in crystallinity is more pronounced, while with increasing fluences the heat exchange during irradiation may induce recrystallisation in HA structure.

Figs. 11 and 12 represent the dependences of *a* and *c* HA unit cell parameters, as well as unit cell volume, on fluence of implanted nitrogen and argon, respectively. The values of unit cell parameters and unit cell volume for non-implanted HA film (which correspond to fluence zero) are given with the aim to compare the results.

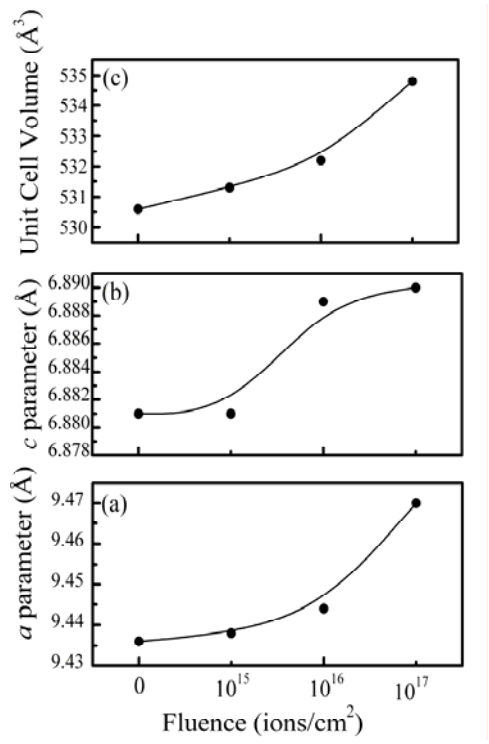

Fig. 11. Dependence of (a) a unit cell parameter, (b) c unit cell parameter, and (c) unit cell volume of HA on implantation fluence of nitrogen ions.

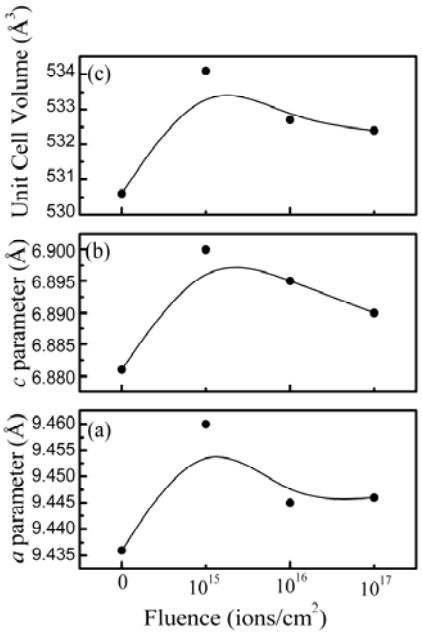

Fig. 12. Dependence of (a) a unit cell parameter, (b) c unit cell parameter, and (c) unit cell volume of HA on implantation fluence of argon ions.

It can be seen from Fig. 11 that unit cell parameters *a* and *c*, as well as unit cell volume of HA, increase with increasing nitrogen ion fluence. Similarly, the unit cell parameters *a* and *c*, as well as unit cell volume of HA, increase after Ar^{6+} ions irradiation to a $1x10^{15}$ ions/cm^2 (Fig. 12). At higher fluences, the unit cell parameters and unit cell volume decrease when argon ion fluences increase to $1x10^{16}$ and $1x10^{17}$ ions/cm^2. These structural changes are consequence of different mechanisms of energy transfer of nitrogen and argon ions to HA film. For nitrogen ion irradiation electron energy loss is predominant, while for argon ion irradiation nuclear energy loss prevails.

4. Conclusions

The effect of nitrogen and argon irradiation on electrophoretically deposited HA thin films on titanium was analyzed and the mechanism of HA surface modification by ion implantation was proposed. The increase in applied fluences decreases the HA crystallite domain size for both implanted ions. In the case of implantation with nitrogen ion, the increase in applied fluences decreases the crystallinity of HA film. In the case of implantation with argon ion, the increase in applied fluences causes initial decrease in crystallinity of HA film followed by further slight increase, i.e. recrystallisation in HA structure. For nitrogen ion irradiation electron energy loss is predominant, while for argon ion irradiation nuclear energy loss prevails.

Acknowledgements

This research was financed by the Ministry of Science and Technological Development, Republic of Serbia, contracts no. 142061 and 142070.

References

[1] I. Braceras, J. I. Alava, L. Goikoetxea, M. A. de Maeztu, J. I. Onate, Surf. Coat. Technol. **201**, 8091 (2007).
[2] A. M. Ektessabi, H. Kimura, Thin Solids Films **270**, 335 (1995).
[3] K. D. Rogers, S. E. Etok, R. Scott, J. Mater. Sci. **39**, 5747 (2004).
[4] V. Nelea, C. Morosanu, M. Iliescu, I. N. Mihailescu, Appl. Surf. Sci. **228**, 346 (2004).
[5] E. Gyorgy, S. Grigorescu, G. Socol, I. N. Mihailescu, Dj. Janackovic, A. Dindune, Z. Kanepe, E. Palcevskis, E. L. Zdrentu, S. M. Petrescu, Appl. Surf. Sci. **253**, 7981 (2007).
[6] H. W. Kim, Y. H. Koh, L. H. Li, S. Lee, H. E. Kim, Biomaterials **25**, 2533 (2004).
[7] L. Pramatarova, E. Pecheva, V. Krastev, J. Mater. Sci: Mater. Med. **18**, 441 (2007).
[8] W. Xu, W. Hu, M. Li, C. Wen, Mater. Lett. **60**, 1575 (2006).
[9] H. Wang, N. Eliaz, Z. Xiang, H. P. Hsu, M. Spector, L. W. Hobbs, Biomaterials **27**, 4192 (2006).
[10] A. Stoch, A. Brożek, S. Błażewicz, W. Jastrzębski, J. Stoch, A. Adamczyk, I. Rój, J. Mol. Structure **651-653**, 389 (2003).
[11] A. Stoch, A. Brożek, G. Kmita, J. Stoch, W. Jastrzębski, A. Rakowska, J. Mol. Structure **596**, 191 (2001).
[12] M. Manso, C. Jiménez, C. Morant, P. Herrero, J. M. Martínez-Duart, Biomaterials **21**, 1755 (2000).
[13] C. Wang, J. Ma, W. Cheng, R. Zhang, Mater. Lett. **57**, 99 (2002).
[14] J. Hamagami, Y. Ato, K. Kanamura, J. Ceram. Soc. Jpn. **114**, 51 (2006).
[15] P. Sarkar, P. S. Nicholson, J. Am. Ceram. Soc. **79**, 1987 (1996).
[16] I. Zhitomirsky, L. Gal-Or, J. Mater. Sci. Mater. Med. **8**, 213 (1997).
[17] C. Kaya, Ceram. Int. **34**, 1843 (2008).
[18] A. M. Ektessabi, Nucl. Instr. and Meth. B **99**, 610 (1995).
[19] S. Prakash Parthiban, R. V. Suganthi, .E. K. Girija, K. Elayaraja, P. K. Kulriya, Y. S. Katharria, F. Singh, I. Sulania, A. Tripathi, K. Asokan, D. Kanjilal, S. Yadav, T. P. Singh, Y. Yokogawa, S. Narayana Kalkura, Nucl. Instr. and Meth. B **266**, 911 (2008).
[20] E. K. Girija, S. P. Parthiban, R. V. Suganthi, K. Elayaraja, M. I. A. Joshy, R. Vani, P. Kularia, K. Asokan, D. Kanjilal, Y. Yokogawa, S. Narayana Kalkura, J. Ceram. Soc. Jpn. **116**, 320 (2008).
[21] H. Pelletier, V. Nelea, P. Mille, D. Muller, Nucl. Instr. and Meth. B **216**, 269 (2004).
[22] H. Pelletier, V. Nelea, P. Mille, D. Muller, Nucl. Instr. and Meth. B **216**, 275 (2004).
[23] J. F. Ziegler, J. P. Biersack, U. Littmark, The Stopping and Range of Ions in Solids, Pergamon Press, code SRIM 2004: (1985) http://www.srim.org.
[24] S. Krumm, Acta Universitatis Carolinae Geologica 38 (1994) 253-261. (version: Beta Relase 1.2.1., June 1997; http://www.geol.uni-erlangem.de)
[25] N. Y. Mostafa, Mater. Chem. Phys. **94**, 333 (2005).
[26] J. S. Williams, Rep. Prog. Phys. **49**, 491 (1986).
[27] M. Ohring, The Materials Science of Thin Films, Academic Press, London, (1991).
[28] N. Bibić, I. H. Wilson, M. Milosavljević, D. Perusko, J. Mater. Sci. **27**, 4945 (1992).
[29] S. Miro, D. Grebille, D. Chateigner, D. Pelloquin, J.-P. Stoquert, J.-J. Grob, J.-M. Constantini, F. Studer, Nucl. Instr. and Meth. B **227**, 306 (2005).

*Corresponding author: vesna@tmf.bg.ac.rs